JOURNAL OF THE ENGINEERING MECHANICS DIVISION

RESPONSE OF TUNNELS TO INCIDENT SH-WAVES

By Vincent W. Lee[1] and Mihailo D. Trifunac,[2] A. M. ASCE

INTRODUCTION

The vibration of a circular underground tunnel excited by SH-waves is investigated in this paper. The exact method of solution involves series expansion of incident and reflected SH-waves in terms of cylindrical wave functions. The solution depends on the material properties of the tunnel and the surrounding medium, on the thickness of the tunnel walls, its depth below the ground surface, and the angle of incident SH-waves. The model response has been characterized by the Fourier amplitudes for steady-state harmonic excitation with unit amplitude. The results thus represent the transfer function amplitudes. This method can be employed to find the exact transient response of circular tunnels subjected to arbitrary transient inputs through Fourier synthesis and for known incident excitation.

The current practice in analyzing the response of underground tunnels often involves an approximate representation of the semi-infinite half space by a finite body surrounding the tunnel (4). Such approximations typically violate the wave propagation aspects of the exact problem and should be tested and verified by comparison with the available exact solutions. The example of a circular tunnel analyzed in this paper can be used for construction and verification of approximate numerical techniques.

The results in this paper show that considerable fluctuations in response amplitudes on ground surface and in the vicinity of the tunnel are possible over short distances. These amplitude fluctuations increase as the tunnel depth decreases and appear to be caused by wave interference between the tunnel wells and the stress-free ground surface. The analysis of stress amplitudes along the tunnel's circumference shows large fluctuations that are governed by the angle of incidence of SH-waves.

[1] Grad. Student, Dept. of Civ. Engrg., Univ. of Southern California, Los Angeles, Calif.

[2] Assoc. Prof., Dept. of Civ. Engrg., Univ. of Southern California, Los Angeles, Calif.

MODEL, EXCITATION, AND SOLUTION OF PROBLEM

   The cross section of the two-dimensional model studied in this paper is shown in Fig. 1. It represents a half space in which a circular cylindrical tunnel of outer radius a is situated. The wall of the tunnel is of thickness ta, in which $0 < t < 1$, the inner radius being $b = (1 - t)a$. The axis of the cylinder is at a depth, D, below the ground surface. The material properties of the elastic isotropic homogeneous half space are characterized by the rigidity, μ_0,
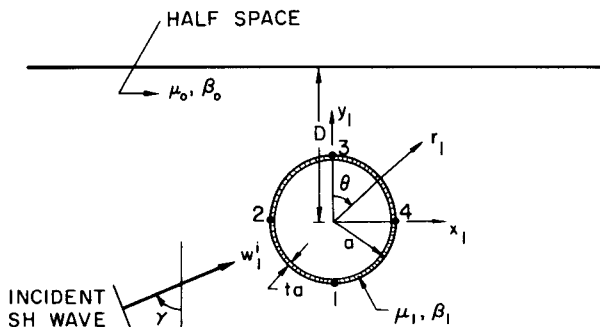
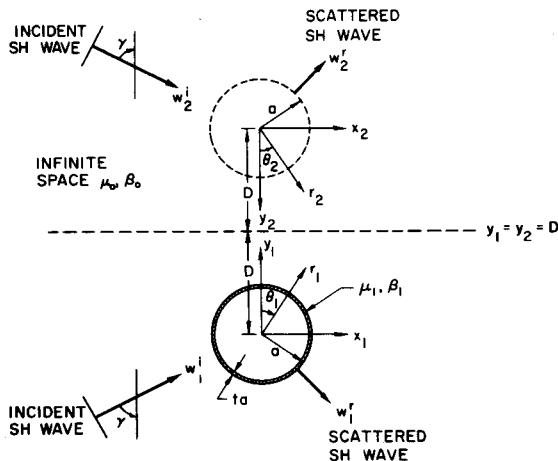FIG. 1.—Underground Circular Tunnel

FIG. 2.—Mathematical Model

and velocity of shear waves, β_0, while that of the tunnel wall are μ_1 and β_1. The two coordinate systems are introduced as: Cartesian coordinate system (x_1, y_1) and polar coordinate system (r_1, θ_1) having common origin at the center of the tunnel (Fig. 1).

   The excitation of the half space, $w_1^{(i)}$, is assumed to consist of an infinite train of plane SH-waves with frequency ω and particle motion in the z direction (Fig. 1) in the half space ($y_1 \leq D$). It is represented by

$$w_1^{(i)} = w_1^{(i)}(r_1, \theta_1) = \exp i \left[\omega t - kr_1 \cos (\theta_1 - \gamma) \right] \quad \ldots \ldots \ldots \ldots \ldots \quad (1)$$

in which $k = \omega / \beta$. This corresponds to a wave with incidence angle γ of amplitude 1, and wavelength $\lambda = 2\pi / k$.

The incident waves, $w_1^{(i)}$, are reflected from the plane free surface ($y_1 = D$), and scattered and diffracted by the outer surface of the tunnel ($r_1 = A$). The resultant total displacement field, $w^{(t)}$, is then a superposition of the incident, reflected, and diffracted waves. Waves are also refracted into the linings of the tunnel. This motion is denoted by $w^{(f)}$. Both $w^{(t)}$ and $w^{(f)}$ must satisfy the differential equation

$$\frac{\partial^2 w}{\partial r_1^2} + \frac{1}{r_1} \frac{\partial w}{r_1} + \frac{1}{r_1^2} \frac{\partial^2 w}{\partial \theta_1^2} = \frac{1}{\beta^2} \frac{\partial^2 w}{\partial t^2} \quad \ldots \ldots \ldots \ldots \ldots \quad (2)$$

in which $w = w^{(t)}$ and $\beta = \beta_0$ in the elastic half space; and $w = w^{(f)}$ and $\beta = \beta_1$ in the elastic lining of the tunnel.

The boundary conditions are, for traction free at $y_1 = D$, the free surface:

$$\sigma_{yz} = \mu_0 \frac{\partial w^{(t)}}{\partial y_1} = 0 \quad \ldots \ldots \ldots \ldots \ldots \ldots \ldots \ldots \quad (3)$$

for continuity of displacement at $r_1 = a$:

$$w^{(t)} = w^{(f)} \quad \ldots \ldots \ldots \ldots \ldots \ldots \ldots \ldots \ldots \quad (4)$$

for continuity of stress at $r_1 = a$:

$$\mu_0 \frac{\partial w^{(t)}}{\partial r_1} = \mu_1 \frac{\partial w^{(f)}}{\partial r_1} \quad \ldots \ldots \ldots \ldots \ldots \ldots \ldots \quad (5)$$

for traction free at $r_1 = b$, the inner radius of the tunnel:

$$\sigma_{rz} = \mu_1 \frac{\partial w^{(f)}}{\partial r_1} = 0 \quad \ldots \ldots \ldots \ldots \ldots \ldots \ldots \quad (6)$$

To solve the problem, we consider an unbounded medium and suppose there is another cylindrical tunnel of radius a with axis at $(x_1, y_1) = (0, 2D)$ (Fig. 2). One can then introduce two additional coordinate systems: the Cartesian coordinate system (x_2, y_2) and the polar coordinate system (r_2, θ_2), having a common origin at the center of the new tunnel as shown in Fig. 2.

Let there be another incident plane SH-wave, $w_2^{(i)}$, given by

$$w_2^{(i)} = w_2^{(i)}(r_2, \theta_2) = \exp i \left[\omega t - kr_2 \cos (\theta_2 - \gamma) \right] \quad \ldots \ldots \ldots \ldots \ldots \quad (7)$$

with respect to the coordinate system (r_2, θ_2).

We assume the waves $w_1^{(r)}$ and $w_2^{(r)}$ that are scattered from and diffracted around the bottom and top tunnels to be represented, respectively, by

$$w_1^{(r)} = w_1^{(r)}(r_1, \theta_1) = \sum_{m=0}^{\infty} H_m^{(2)}(kr_1)(A_m \cos m\theta_1 + B_m \sin m\theta_1) \exp (i\omega t) \qquad (8)$$

$$w_2^{(r)} = w_2^{(r)}(r_2, \theta_2) = \sum_{m=0}^{\infty} H_m^{(2)}(kr_2)(A_m \cos m\theta_2 + B_m \sin m\theta_2) \exp (i\omega t) \qquad (9)$$

relative to their respective coordinate systems. We will omit the time factor $\exp(i\omega t)$ from now on. The Hankel functions of the second kind $H_m^{(2)}(\cdot)$ are chosen because they correspond to outgoing cylindrical waves.

In the unbounded medium, the derivatives with respect to y_1 of $w_1^{(i)} + w_2^{(i)}$, and $w_1^{(r)} + w_2^{(r)}$ each vanish at $y_1 = D$ because of the symmetry of their representation with respect to $y_1 = y_2 = D$. Thus, in the half space $y_1 \le D$, the sum of the displacement fields, $w_1^{(i)} + w_2^{(i)}$ and $w_1^{(r)} + w_2^{(r)}$, together satisfies the wave equation, Eq. 2, as well as the traction-free condition (Eq. 3) at $y_1 = D$. The resulting displacement field, in the elastic half space, $w^{(t)}$, is

$$w^{(t)} = w_1^{(i)} + w_2^{(i)} + w_1^{(r)} + w_2^{(r)} \ \ldots\ldots\ldots\ldots (10)$$

The resulting displacement field in the elastic lining of the tunnel, $w^{(f)}$, satisfying the wave equation, Eq. 2, can be written as

$$w^{(f)} = w^{(f)}(r_1,\theta_1) = \sum_{m=0}^{\infty} + \begin{array}{l} [C_m^{(1)} H_m^{(1)}(k_1 r_1) + C_m^{(2)} H_m^{(2)}(k_1 r_1)]\ \cos m\theta_1 \\ [D_m^{(1)} H_m^{(1)}(k_1 r_1) + D_m^{(2)} H_m^{(2)}(k_1 r_1)]\ \sin m\theta_1 \end{array} \quad (11)$$

in which $k_1 = \omega/\beta_1$, $H^{(1)}(\cdot)$ and $H^{(2)}(\cdot)$ being the Hankel functions of the first and second kind, respectively. The values $w^{(t)}$ and $w^{(f)}$ must satisfy the boundary conditions in Eqs. 4, 5, and 6.

Applying Eq. 6 to $w^{(f)}$ at $r_1 = b$, the inner radius

$$\sum_{m=0}^{\infty} + \begin{array}{l} [C_m^{(1)} H_m'^{(1)}(k_1 r_1) + C_m^{(2)} H_m'^{(2)}(k_1 r_1)]\ \cos m\theta_1 \\ [D_m^{(1)} H_m'^{(1)}(k_1 r_1) + D_m^{(2)} H_m'^{(2)}(k_1 r_1)]\ \sin m\theta_1 = 0 \end{array} \quad \text{at} \ \ r_1 = b \ \ldots\ (12)$$

$$\text{or} \quad C_m^{(1)} = -C_m^{(2)} \left. \frac{H_m'^{(2)}(k_1 r_1)}{H_m'^{(1)}(k_1 r_1)}\right|_{r_1=b} \ \ldots\ldots\ldots\ldots (13)$$

$$\text{and} \quad D_m^{(1)} = -D_m^{(2)} \left. \frac{H_m'^{(2)}(k_1 r_1)}{H_m'^{(1)}(k_1 r_1)}\right|_{r_1=b} \ \ldots\ldots\ldots\ldots\ldots (14)$$

in which prime in $H_m'(\cdot)$ denotes differentiation with respect to argument.

By eliminating $C_m^{(1)}$ and $D_m^{(1)}$ in Eq. 11

$$w^{(f)} = \sum_{m=0}^{\infty} G_m(k_1 r_1)(C_m^{(2)} \cos m\theta_1 + D_m^{(2)} \sin m\theta_1) \ \ldots\ldots\ldots\ldots (15)$$

in which for $b > 0$: $\quad G_m(k_1 r_1) = H_m^{(2)}(k_1 r_1)$

$$-\left. \frac{H_m'^{(2)}(k_1 r_1)}{H_m'^{(1)}(k_1 r_1)}\right|_{r=b} H_m^{(1)}(k_1 r_1) \ \ldots\ldots\ldots\ldots\ldots (16)$$

For the case $b = 0$, the analysis applies with $G_m(k_1 r_1) = J_m(k_1 r_1)$.

Boundary conditions 4 and 5 correspond to the continuity of displacement and stress at the outer radius $r_1 = a$. To apply conditions 4 and 5, we first transform $w_2^{(i)}$ (Eq. 7) and $w_2^{(r)}$ (Eq. 9) to the (r_1, θ_1) coordinates. Eq. 9 can be rewritten as

$$w_2^{(i)} = w_2^{(i)}(r_1,\theta_1) = \exp[-i2kD \cos\gamma + ikr_1 \cos(\gamma + \theta_1)] \ \ldots\ldots\ldots (17)$$

For Eq. 9, we use the Addition theorem (1,2,3)

$$H_n^{(2)}(kr_2)\begin{pmatrix} \cos & n\theta_2 \\ \sin & n\theta_2 \end{pmatrix} = \sum_{m=-\infty}^{\infty} J_m(kr_1) H_{n+m}^{(2)}(2kD)\begin{pmatrix} \cos & m\theta_1 \\ \sin & m\theta_1 \end{pmatrix} \quad \cdots \cdots \quad (18)$$

$$H_n^{(2)}(kr_2)\begin{pmatrix} \cos & n\theta_2 \\ \sin & n\theta_2 \end{pmatrix} = \sum_{m=0}^{\infty} J_m(kr_1)\begin{pmatrix} P_{mn}^+(2kD) & \cos m\theta_1 \\ P_{mn}^-(2kD) & \sin m\theta_1 \end{pmatrix};$$

$$n = 0, 1, 2, \ldots \quad \cdots \cdots \cdots \cdots \cdots \cdots \cdots \cdots \cdots \cdots \cdots \quad (19)$$

in which $\quad P_{mn}^\pm(2kD) = \dfrac{\epsilon_m}{2} [H_{n+m}^{(2)}(2kD) \pm H_{n-m}^{(2)}(2kD)] \quad \cdots \cdots \cdots \quad (20)$

and $\quad \epsilon_0 = 1, \ \epsilon_m = 2 \quad$ for $\quad m > 1; \quad n, m = 0, 1, 2, \ldots \cdots \cdots \cdots \cdots \quad (21)$

Eq. 9 can then be rewritten as

$$w_2^{(r)} = w_2^{(r)}(r_1, \theta_1) = \sum_{m=0}^{\infty} J_m(kr_1)(A_m^* \cos m\theta_1 + B_m^* \sin m\theta_1) \quad \cdots \cdots \cdots \quad (22)$$

in which $\quad A_m^* = \displaystyle\sum_{n=0}^{\infty} P_{mn}^+(2kD) A_n;$

and $\quad B_m^* = \displaystyle\sum_{n=0}^{\infty} P_{mn}^-(2kD) B_n; \quad m = 0, 1, 2, \ldots \cdots \cdots \cdots \cdots \cdots \quad (23)$

Next, $w_1^{(i)}$ and $w_2^{(i)}$ are expressed in terms of Bessel's functions, so that

$$w_1^{(i)} = w_1^{(i)}(r_1, \theta_1) = \sum_{m=0}^{\infty} \epsilon_m(-i)^m J_m(kr_1)(\cos m\gamma \cos m\theta_1$$

$$+ \sin m\gamma \sin m\theta_1) \quad \cdots \cdots \cdots \cdots \cdots \cdots \cdots \cdots \cdots \cdots \quad (24)$$

$$w_2^{(i)} = w_2^{(i)}(r_1, \theta_1)$$

$$= \exp(-i2kD\cos\gamma) \sum_{m=0}^{\infty} \epsilon_m i^m J_m(kr_1)\begin{pmatrix} - & \cos m\gamma \cos m\theta_1 \\ & \sin m\gamma \sin m\theta_1 \end{pmatrix} \quad \cdots \cdots \cdots \quad (25)$$

Using Eqs. 8, 11, 22, 24, 25 and boundary conditions 4 and 5 gives, at $kr_1 = ka$

$$\frac{A_m H_m^{(2)'}}{J_m} + A_m^* + \epsilon_m [(-i)^m + \exp(-i2kD\cos\gamma) i^m] \cos m\gamma$$

$$= \left(\frac{\mu_1}{\mu_0}\right) C_m^{(2)} \frac{G_m'}{J_m'} \quad \cdots \cdots \cdots \cdots \cdots \cdots \cdots \cdots \cdots \quad (26)$$

$$\frac{A_m H_m^{(2)'}}{J_m} + A_m^* + \epsilon_m [(-i)^m + \exp(-i2kD\cos\gamma) i^m] \cos m\gamma$$

$$+ C_m^{(2)} \frac{G_m}{J_m} \quad \cdots \cdots \cdots \cdots \cdots \cdots \cdots \cdots \cdots \cdots \cdots \quad (27)$$

Simplifying Eqs. 26 and 27 gives

$$C_m^{(2)} = R_m(ka) A_m \quad \dots \dots \dots \dots \dots \dots \dots \dots \dots \dots \quad (28)$$

in which

$$R_m(ka) = \left. \frac{\dfrac{H_m^{(2)}}{J_m} - \dfrac{H_m^{(2)\prime}}{J_m'}}{\dfrac{G_m}{J_m} - \dfrac{\mu_1}{\mu_0}\dfrac{G_m'}{J_m'}} \right|_{r_1 = a} \quad \dots \dots \dots \dots \quad (29)$$

and

$$\left. \frac{H_m^{(2)} - R_m G_m}{J_m} \right|_{r_1 = a} A_m + \sum_{h=0}^{\infty} P_{mn}^+ A_n$$

$$= -\epsilon_m \left[(-i)^m + \exp\left(-i2kD\cos\gamma\right) i^m \right] \cos m\gamma ; \quad m = 0, 1, 2, \dots \quad \dots \quad (30)$$

Similarly, we have for B_m

$$D_m^{(2)} = R_m(ka) B_m \quad \dots \dots \dots \dots \dots \dots \dots \dots \dots \dots \quad (31)$$
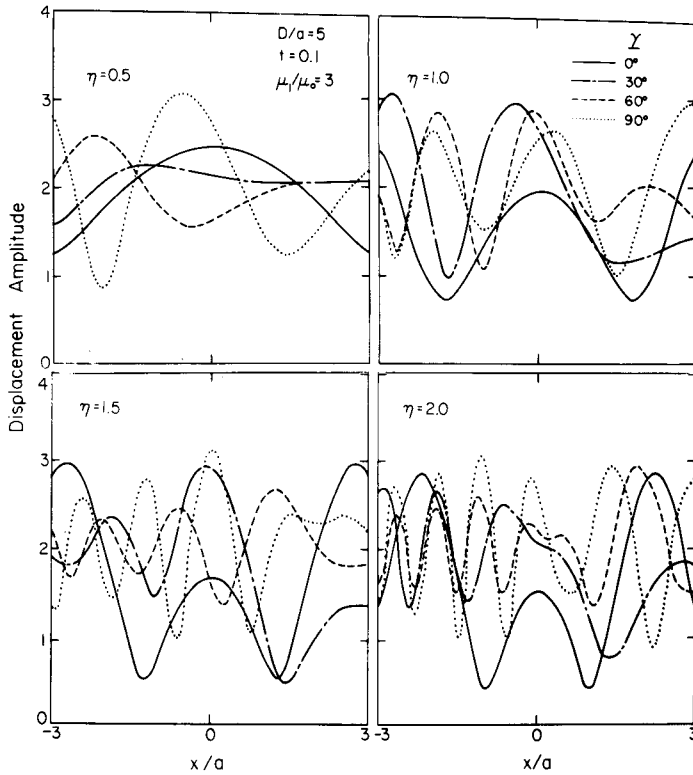

FIG. 3.—Surface Displacement Amplitudes for $\eta = 0.5$, 1.0, 1.5, and 2.0 and for $D/a = 5$, $t = 0.1$, and $\mu_1/\mu_0 = 0.35$

$$\frac{H_m^{(2)} - R_m G_m}{J_m}\Bigg|_{r_1=a} B_m + \sum_{n=1}^{\infty} P_{mn}^- B_n$$

$$= -\epsilon_m [(-i)^m - \exp(-i2kD\cos\gamma)\, i^m]\, \sin m\gamma \, ; \quad m = 0, 1, 2, \dots \dots \quad (32)$$

Eqs. 30 and 32 each constitute an infinite matrix for the unknown coefficients A_m, B_m, $m = 0, 1, 2, \dots$, $(B_0 = 0)$. Such a matrix equation of infinite order can be approximated by one of finite order. The truncated series than represents low frequency position of the exact solution.
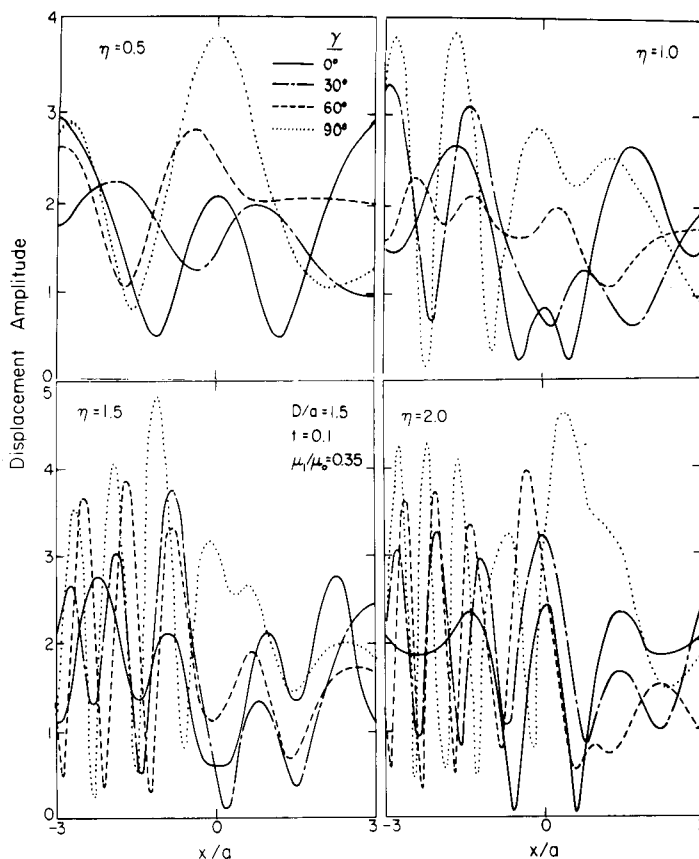

FIG. 4.—Surface Displacement Amplitudes for $\eta = 0.5$, 1.0, 1.5, and 2.0 and for $D/a = 5$, $t = 0.1$, and $\mu_1/\mu_0 - 3$

For the case $\mu_1 = 0$, the case of a cavity of radius a in an elastic half space, the term, $H_m^{(2)} - R_m G_m/J_m$, in Eqs. 30 and 32 reduces to $H_m^{(2)'}/J_m'$ and Eqs. 30 and 32 reduce to equations for the case of a cavity first derived in Ref. 1.

SURFACE DISPLACEMENT AND STRESS AMPLITUDES

For the seismological and earthquake engineering applications, a useful aspect of the preceding analysis is the description of the displacement amplitudes along

the surface of the half space above and near the tunnel, and displacement and stress amplitudes on the surface of the tunnel itself.

For the plane SH-wave excitation with amplitude 1, the resulting motion can be characterized by the modulus, or displacement amplitude

$$\text{displacement amplitude} \equiv |w| \equiv [\text{Re}^2(w') + \text{Im}^2(w')]^{1/2} \quad \ldots \ldots \ldots \ldots \quad (33)$$

In the absence of the tunnel, the modulus of ground displacement in the uniform half space is equal to 2. In the presence of the tunnel, waves are

FIG. 5.—Surface Displacement Amplitudes for η = 0.5, 1.0, 1.5, and 2.0 and for D/a = 1.5, t = 0.1, and μ_1/μ_0 = 0.35

scattered and diffracted around the tunnel, and the resulting modulus may depart significantly from 2.

Similarly, the resultant stress of interest, σ_{rz}, on the surface of the tunnel can be characterized by the normalized stress amplitude, σ^*, given by

$$\sigma^* \equiv \frac{\left.\dfrac{\partial w^t}{\partial r_1}\right|_{r_1=a}}{k} \equiv \frac{\mu_1 \left.\left|\dfrac{\partial w^f}{\partial r_1}\right|\right|_{r_1=a}}{\mu_0 k} \quad \ldots \ldots \ldots \ldots \ldots \ldots \ldots \ldots \quad (34)$$

in which $\mu_0 k = \mu_0 \omega/\beta = \mu_0 |\partial w^i/\partial r|$ corresponds to the stress amplitude

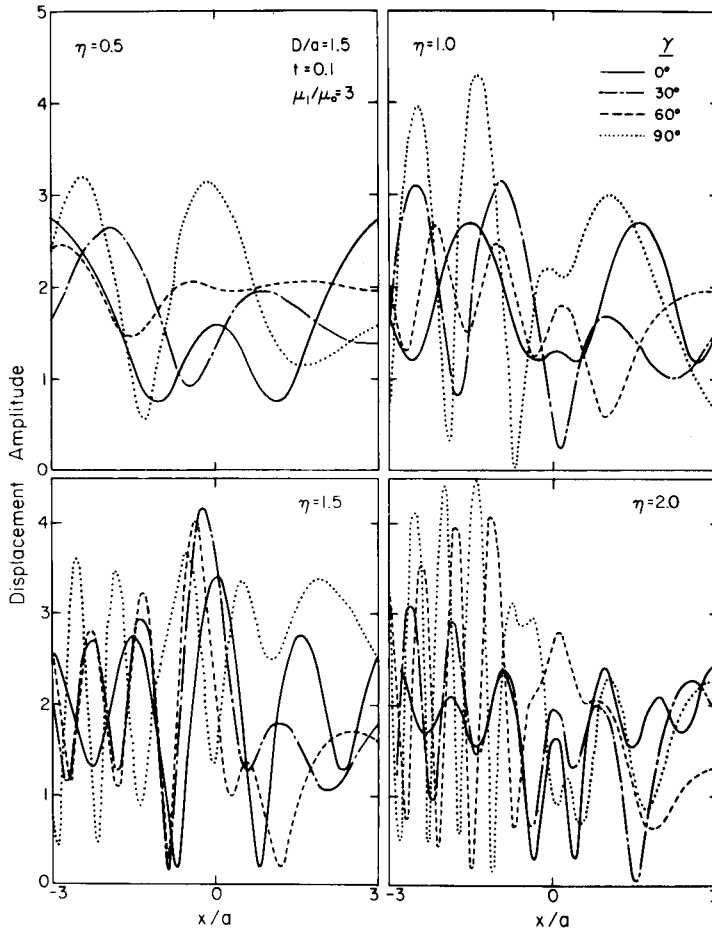FIG. 6.—Surface Displacement Amplitudes for $\eta = 0.5$, 1.0, 1.5, and 2.0 and for $D/a = 1.5$, $t = 0.1$, and $\mu_1/\mu_0 = 3$

of the input SH-wave. The presence and the proximity of the half-space boundary will significantly affect the displacement and stress amplitudes on the surface of the tunnel.

Figs. 3 and 4 present examples of displacement amplitudes plotted versus x/a on the surface ($y_1 = D$) and for $\eta = 0.5$, 1.0, 1.5, and 2.0; $D/a = 0.5$;
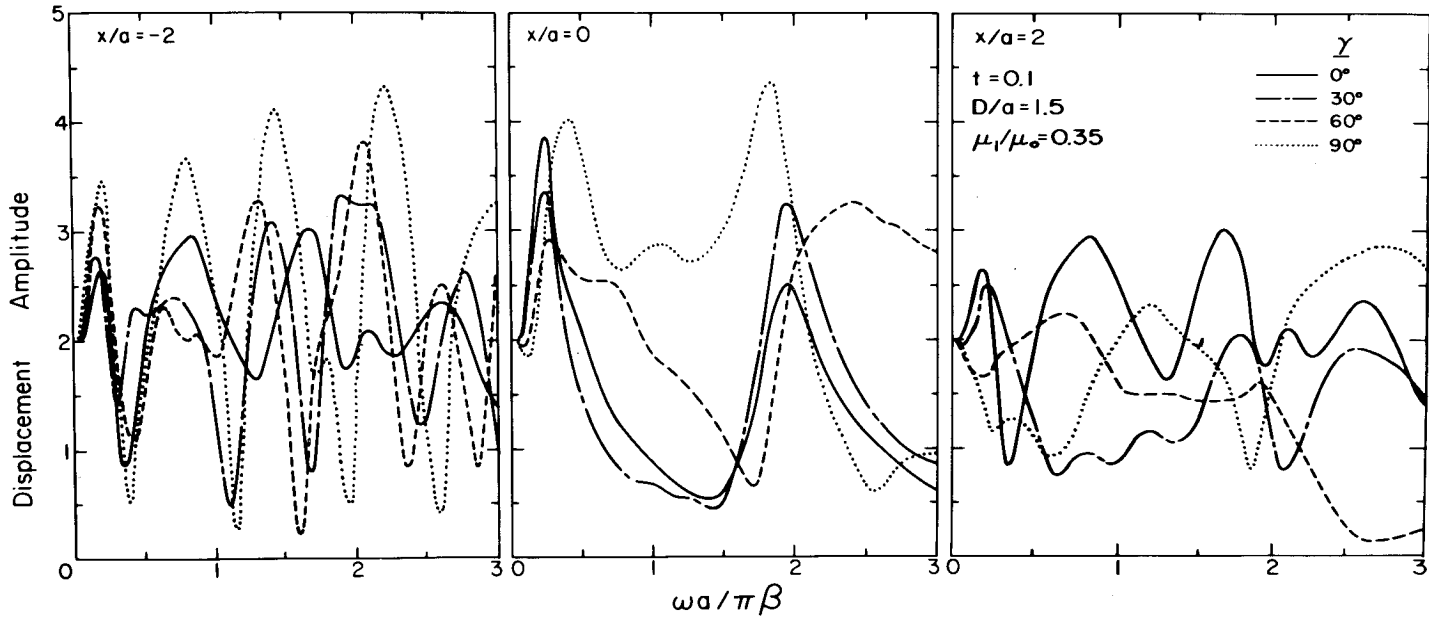
FIG. 7.—Surface Displacement Amplitudes versus Frequency at $x/a = -2$, 0, and 2 and for $t = 0.1$, $D/a = 1.5$, and $\mu_1/\mu_0 = 0.35$
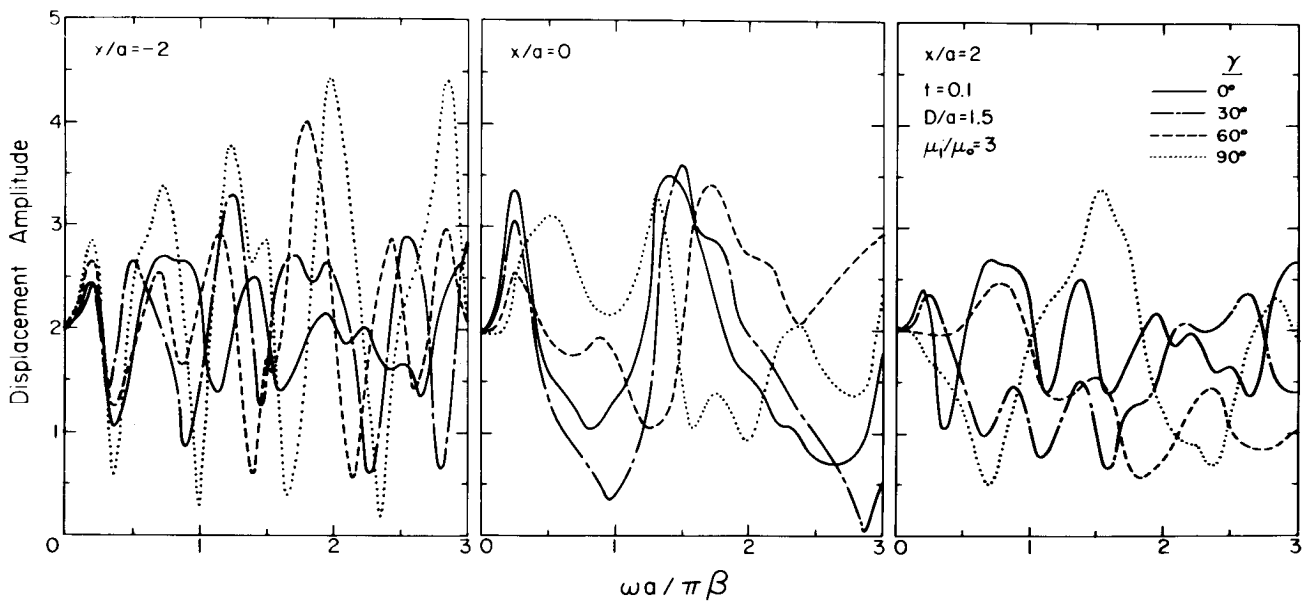
FIG. 8.—Surface Displacement Amplitudes Versus Frequency at $x/a = -2$, 0, and 2 and for $t = 0.1$, $D/a = 1.5$, and $\mu_1/\mu_0 = 3$

$t = 0.1$; and $\mu_1/\mu_0 = 0.35$ and 3.0. These examples correspond to a deep tunnel of rigidity which is one-third and three times the rigidity of the surrounding elastic half space. For vertical incidence of SH-waves, $\gamma = 0$, surface displacement amplitudes are symmetric with respect to $x/a = 0$. As γ increases towards 90° the complexity of motion increases more for $x/a < 0$ than for $x/a >$
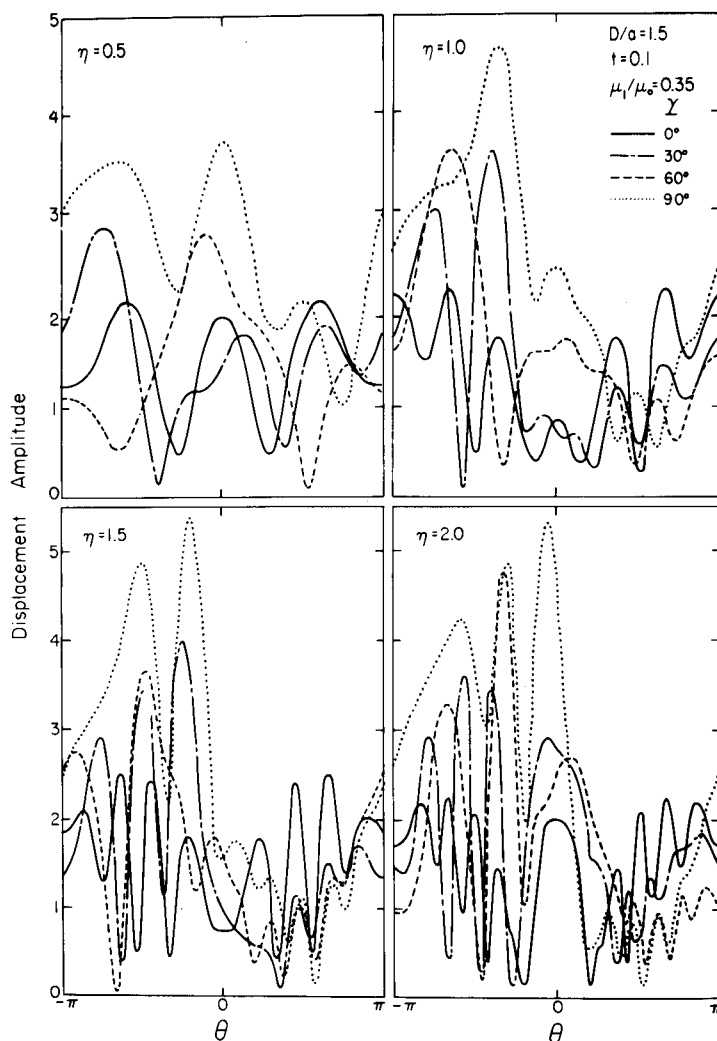

FIG. 9.—Displacement Amplitudes of Tunnel Wall for $\eta = 0.5$, 1.0, 1.5, and 2.0 and for $D/a = 1.5$ and $\mu_1/\mu_0 = 0.35$

0 because of the interference of incident and the waves scattered from the tunnel. The displacement amplitudes in these figures oscillate about the mean level equal to 2. The shadow zone behind the tunnel is only weakly observed, e.g., for $\gamma = 30$, $\eta = 1.0$, and $\mu_1/\mu_0 = 0.35$. For μ_1/μ_0 the rigid tunnel

is more efficient in transmitting the incident wave energy to medium behind the tunnel. Consequently, this shadow zone essentially disappears for μ_1/μ_0 = 3 in Fig. 4. In general, the rigidity of the tunnel appears to play a secondary role in influencing the surface displacement amplitudes when $D/a = 5$.

Figs. 5 and 6 present the corresponding examples except for $D/a = 1.5$, i.e., a shallow tunnel. The shadow zone for $\eta = 1.0$ and $\gamma = 0°$ and $30°$ now becomes more prominent for $\mu_1/\mu_0 = 0.35$. However, for $\mu_1/\mu_0 = 3$, as in the foregoing example, the stiff tunnel (Fig. 6) essentially eliminates this
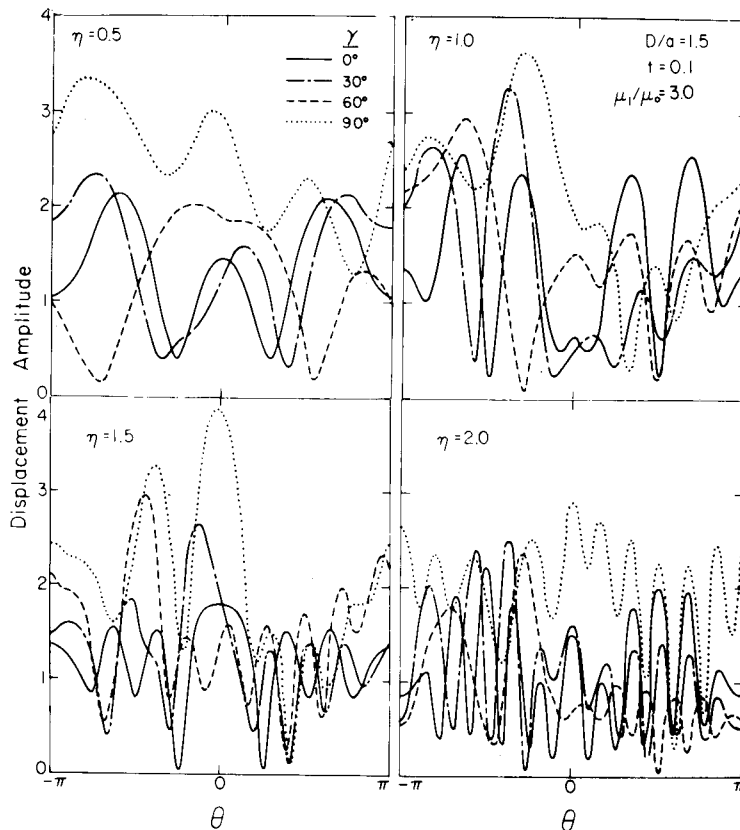

FIG. 10.—Displacement Amplitudes of Tunnel Wall for η = 0.5, 1.0, 1.5, and 2.0 and for D/a = 1.5, t = 0.1, and μ_1/μ_0 = 3.0

shadow zone by driving the medium between $y_1 = D$ and $r_1 = a$ with energy generated by incident waves on the bottom and left walls of the tunnel. For larger values of η (shorter incident waves) and for larger γ (near 90) the complexity of interference patterns in Figs. 5 and 6 increases considerably relative to the corresponding examples in Figs. 3 and 4. The shallow tunnel ($D/a = 1.5$) now acts as a more efficient shallow barrier that scatters most of the incident SH-wave energy back towards $x/a < 0$. As a result surface displacement amplitudes

display rapid fluctuations between 0 and 4 and suggest strong participation of standing wave patterns in the total ground motion. Figs. 7 and 8 show the transfer function spectral amplitudes plotted versus $\omega a/\pi\beta$ at $x/a = -2$, 0, and 2 for $t = 0.1$, $D/a = 1.5$, and for $\mu_1/\mu_0 = 0.35$ and 3, respectively.
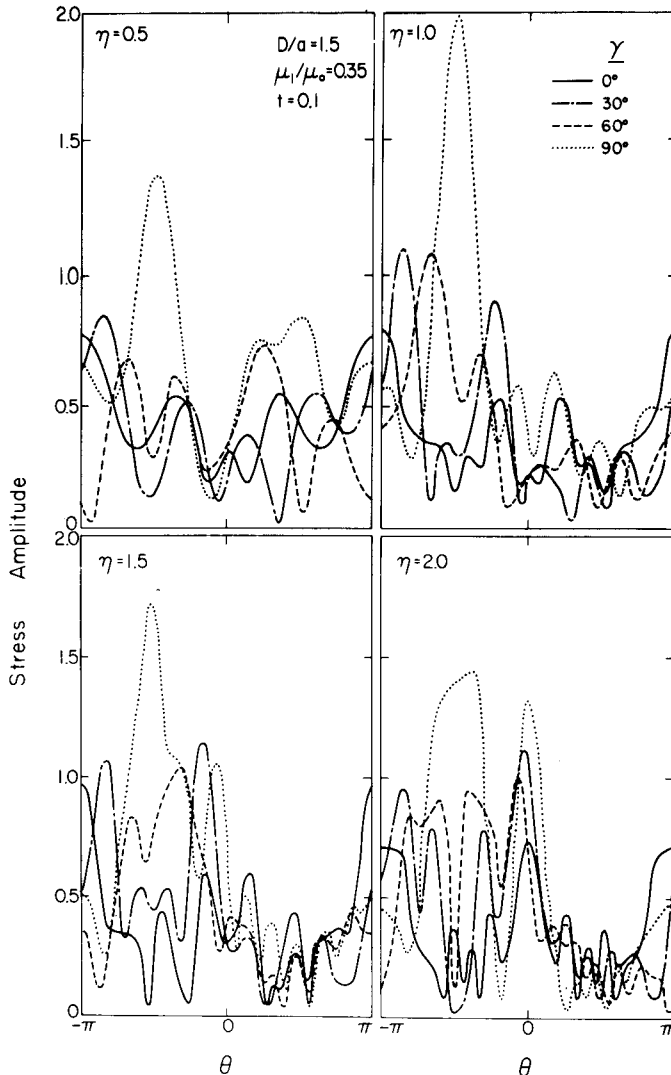

FIG. 11.—Normalized Stress Amplitudes at Outer Tunnel Surface for $\eta = 0.5$, 1.0, 1.5, and 2.0 and for $D/a = 1.5$, $\mu_1/\mu_0 = 0.35$, and $t = 0.1$

As already seen in Figs. 3, 4, 5, and 6, for $x/a < 0$, displacement amplitudes display larger and more abrupt fluctuations than for $x/a > 0$.

Figs. 9, 10, 11, and 12 show the changes of displacement amplitudes and

normalized stress amplitudes with respect to θ, for $D/a = 1.5$, $\mu_1/\mu_0 = 0.35$ and 3, $t = 0.1$, and $\eta = 0.5$, 1.0, 1.5, and 2.0. It is seen that the more flexible tunnel experiences larger and more rapidly fluctuating displacements, but is subjected to smaller stresses than the more rigid canyon (Figs. 10 and 12),
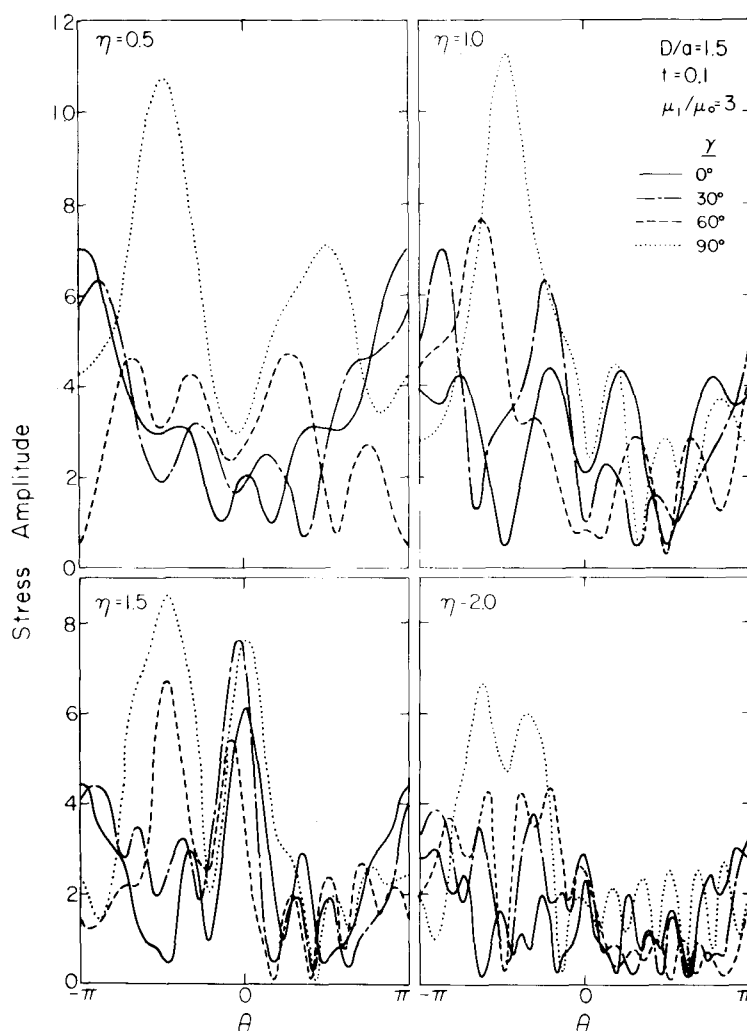

FIG. 12.—Normalized Stress Amplitudes at Outer Tunnel Surface for $\eta = 0.5$, 1.0, 1.5, and 2.0 and for $D/a = 1.5$, $\mu_1/\mu_0 = 3$, and $t = 0.1$

for $\mu_1/\mu_0 = 3$. For greater μ_1 the tunnel wall is more efficient in averaging displacement amplitudes along its circumference but at the same time, "attracts" higher stresses.

Conclusions

Certain aspects of the exact solution of the vibrations of an elastic tunnel embedded in elastic half space and subjected to incident plane SH-waves have been presented herein. The practical engineering uses of the theory presented in this work are, of course, severely limited by the simplicity of the geometrical characteristics of the model considered. The physical insights into the nature of wave scattering, diffraction, and interference in this problem should, however, be of considerable value for the development of improved approximate solution techniques. For proper development and testing of approximate solution methods, it is necessary to consider all physical phenomena present in a problem of this type and to have an exact solution to critically compare with an approximate representation. Different mathematical and physical approximations are often analogous to adding or deleting certain spurious wave sources and unless it is possible to compare results with an exact representation, it is difficult to evaluate such approximate methods. The examples presented in this paper show that the scattered field from the tunnel does not attenuate quickly ($\sim 1/\sqrt{r}$) with distance away from its axis. This means that in those approximate representations, which involve finite element or finite difference "box" surrounding the tunnel, particular care must be taken to eliminate the back scattering of these waves by the boundaries of the box.

Acknowledgments

Appendix I.—References

1. Lee, V. W., "On Deformations Near Circular Underground Cavity Subjected to Incident Plane SH-waves," *Proceedings of the Application of Computer Methods in Engineering Conference*, Vol. II, University of Sourthern California, Los Angeles, Calif., 1977, pp. 951–962.
2. Morse, P. M., and Feshbach, H., *Methods of Theoretical Physics*, McGraw-Hill Book Co., Inc., New York, N.Y., 1953.
3. Mow, C. C., and Pao, Y. H., "The Diffraction of Elastic Waves and Dynamic Stress Concentration," *RAND Report R-482-PR*, Rand Corp., Santa Monica, Calif., 1971.
4. Okamoto, S., *Introduction to Earthquake Engineering*, Halsted Press, Toronto, Canada, 1973.

Appendix II.—Notation

The following symbols are used in this paper:

$$
\begin{aligned}
A_m, B_m, C_m, D_m &= \text{complex coefficients;} \\
a, b &= \text{outer and inner radii of tunnel;} \\
D &= \text{depth of axis of cylinder below ground surface;} \\
H_m^{(1)}(\cdot), H_m^{(2)}(\cdot) &= \text{Hankel functions of first and second kind of order } m; \\
J_m(\cdot) &= \text{Bessel functions of first kind of order } m;
\end{aligned}
$$

$k = \omega/\beta_0$ = wave number in soil;

$k_1 = \omega/\beta_1$ = wave number in the tunnel;

r_1, r_2 = radial distances in polar coordinates;

t = ratio of thickness of tunnel's lining and outer radius;

$w^{(f)}$ = refracted displacement in tunnel's lining;

$w_1^{(i)}, w_2^{(i)}$ = displacement due to incident SH-waves;

$w_1^{(r)}, w_2^{(r)}$ = displacement due to scatter SH-waves;

$w^{(t)}$ = resultant total displacement in soil;

$(x_1, y_1), (x_2, y_2)$ = Cartesian coordinate systems;

β_0 = shear wave velocity in soil;

β_1 = shear wave velocity in tunnel;

ϵ_m = $\epsilon_0 = 1$, $\epsilon_m = 2$ for $m > 1$;

γ = angle of incidence of SH-waves;

η = ratio of diameter of tunnel, $2a$ and λ, wavelength of incident SH-waves;

θ_1, θ_2 = azimuth in polar coordinates;

λ = wavelength of incident SH-waves;

μ_0 = rigidity of soil;

μ_1 = rigidity of tunnel;

σ^* = normalized stress amplitude; and

ω = angular frequency.

14749 RESPONSE OF TUNNELS TO INCIDENT SH-WAVES

KEY WORDS: **Displacement;** Interference; Stress; **Transfer functions;**
Tunnels; Waves

ABSTRACT: The two-dimensional scattering and diffraction of plane-state SH-waves
by a circular tunnel in a homogeneous elastic half space has been analyzed. Using the
series solution of the problem for a general angle of wave incidence, stresses and
deformations near the tunnel have been studied. Their amplitudes have been
demonstrated to be dependent upon the following parameters: the angle of incidence,
ratio of the tunnel thickness to its diameter, ratio of the shear moduli of its wall to
that of its surroundings, and the ratio of its depth to its diameter. The incidence angle,
, determines the overall trends of the amplitudes. Higher frequency incident waves
lead to greater complexity of the computed amplitudes. Stiffer tunnel leads to higher
stresses on the outer tunnel surface. Perturbations of surface displacement amplitudes,
which result from wave interference between tunnel and stress-free half-space surface,
diminish with increasing depth of tunnels.